

CrossMark  
click for updatesCite this: *RSC Adv.*, 2015, 5, 56210

## Au@ZnO hybrid nanostructures: correlation between morphology and optical response†

Ezequiel R. Encina, Manuel A. Pérez and Eduardo A. Coronado\*

Au@ZnO hybrid nanostructures (HNs) have been synthesized in aqueous media by implementing a simple chemical methodology. These HNs consist of 40 nm mean size almost spherical Au cores, over which the heterogeneous formation of ZnO is observed. By increasing the concentration of ZnO precursors in the system, it is possible to change the morphology of the material formed over the Au core from branched to shell like structures, which, in turn, significantly modifies the extinction properties of the naked Au core nanoparticles. This effect has been rationalized by means of electrodynamics simulations based on two different approaches: the Mie theory for coated spheres and the Discrete Dipole Approximation (DDA). The changes measured in the extinction spectra as the amount of ZnO formed around the Au cores increases are properly described by both methodologies, while the good correlation between experimental and theoretical spectra suggest that the ZnO material includes a significant amount of water. Furthermore, based on the Mie theory results, a graphical method was implemented which allows us to predict the main morphological parameters of the Au@ZnO HNs. In addition, the combination of optical measurements, morphological characterization and DDA modeling allowed us to estimate that the water content of the shell surrounding the metallic core is 65%. The methodology presented in this work provides a useful tool to characterize the structural properties of HNs and can be straightforwardly generalized to other systems.

Received 1st April 2015  
Accepted 18th June 2015

DOI: 10.1039/c5ra05834a

www.rsc.org/advances

## Introduction

Hybrid nanostructures (HNs) composed of noble metal and semiconductor materials are currently materials of great interest as this particular kind of system may exhibit novel and unique physical chemistry properties, achieving potential applications in diverse areas such as biological detection, catalysis and solar energy conversion.<sup>1–6</sup> Regarded separately, the optical properties of noble metal (NPs) and semiconductor (QDs) nanoparticles are characterized by the elusive localized surface plasmon resonances (LSPR) and excitons, respectively. In both cases, the excitation wavelength required to produce such excitations strongly depends on the NP nature, size, shape and local environment.<sup>7–9</sup> Consequently, synthetic methodologies capable to produce NPs and QDs with narrow size and shape distributions are necessary in order to rationally employ the optical properties of nanosized matter in a given device.<sup>10–14</sup> Nonetheless, when considering the optical properties of HNs, it may be different from that observed for NPs and QDs separately as a consequence of the interaction between the respective HNs building blocks. Moreover, the interaction between the

constitutive parts of a given HN can be tuned by controlling the three-dimensional arrangement, size and shape of the HN building blocks. Energy transfer processes may take place if QDs and NPs are located adjacent within a given HN and Förster resonance energy transfer as well as nanometal surface energy transfer mechanisms had been employed to characterize these processes.<sup>15–19</sup> For instance, Viste *et al.* showed the possibility of tuning under control the emission efficiency of HNs for a large range of Au NP sizes and demonstrated that the modification factor of emission of the hybrid nanosources compared to the bare QDs strongly depends on the Au NP size.<sup>20</sup> In addition, interfacial charge transfer processes, which are relevant in photocatalytic reactions and light energy conversion, may also occur if QDs and NPs are close enough.<sup>21–23</sup> In this regard, it has been demonstrated that the photo-generated electron transfer and the resulting catalytic activity of ZnO–Au composites can be controlled by the size of the mediating Au NP.<sup>24</sup>

Several chemical strategies have been developed and implemented to prepare HNs, resulting in a wide variety of different structures with distinct morphology and structural parameters, which, in turn, allow the study of optical phenomena that might result from the interaction between NPs and QDs. Indeed, general growth strategies has been reported for the synthesis of water dispersible Au@X (X = ZnS, AgS, CuS, PbS, CdS, CdSe, CdTe) core shell HNs, which achieves precise control of the morphologies of the structures.<sup>25,26</sup> Au–TiO<sub>2</sub>

INFIQC-CONICET, Departamento de Físicoquímica, Facultad de Ciencias Químicas, Universidad Nacional de Córdoba, Córdoba (5000), Argentina. E-mail: coronado@fcq.unc.edu.ar; Fax: +54-351-433-4180; Tel: +54-351-535-3866

† Electronic supplementary information (ESI) available. See DOI: 10.1039/c5ra05834a

nanocomposites has also been successfully synthesized by several authors.<sup>27</sup> In particular, Au@ZnO HNs with various morphologies have been prepared by different methods. Composites composed by large ZnO domains (several hundreds of nm) decorated with Au NPs likely comprise the kind of Au–ZnO HN most described in literature.<sup>28</sup> Nonetheless, Haldar *et al.* have implemented a simple method to prepare water soluble and stable Au@ZnO core shell HNs in the size range below 10 nm.<sup>29</sup> More recently, the synthesis of Au@ZnO HNs with a novel hexagonal pyramid-like structure has also been reported.<sup>30</sup> However, to the best of our knowledge, reports concerning the preparation of Au@ZnO core shell HNs are rare.

On the other hand, the employment of theoretical approaches to describe the optical properties of HNs is of great importance to achieve a better understanding of the observed phenomena. For instance, an analytical model based on an approximate Mie's theory has been employed to study the optical features of Au@Cu<sub>2</sub>O core shell HNs prepared by controlling epitaxial growth of Cu<sub>2</sub>O on as-prepared Au NPs in aqueous solution.<sup>31</sup> Wang and co-workers applied the Mie theory for coated spheres to interpret the complexity of extinction spectral line shapes and geometry-dependent optical tunability of the Au@Cu<sub>2</sub>O HNs.<sup>32</sup> More recently, these authors employed the Mie theory for coated spheres along with effective medium theory to achieve a quantitative understanding of the geometry-dependent optical tunability of Au@Cu<sub>2</sub>O HNs with porous Cu<sub>2</sub>O shells.<sup>33</sup> The same theoretical approach has been employed to reveal the growth mechanism in Ag@ZnO core shell HNs.<sup>34</sup> The Mie theory and the four-flux method has been applied to study theoretically the influence of an oxide (SiO<sub>2</sub>, ZnO<sub>2</sub>, or TiO<sub>2</sub>) shell on a metal core (Ag, Au, or Cu) NP.<sup>35</sup> Shaviv *et al.* studied the light absorption properties of CdS–Au and CdSe–Au HNs by comparing experimental results with electro-dynamics simulations obtained by applying the DDA method.<sup>36</sup> In this case, a qualitative agreement between DDA simulations and experimental data for CdS–Au HNs has been found and it has been stated that DDA simulations provide insights on the gold tip shape and its interface with the semiconductor material. For the CdSe–Au case, a shortcoming of the electro-dynamics model was found, as it does not predict properly the optical features, which was ascribed to strong interaction of the metal and semiconductor excitations, that spectrally overlap in the CdSe case. However, as far as we know, the employment of electro-dynamics simulations to obtain further insight on the optical properties of Au@ZnO HNs has not been reported so far.

In this work, a simple chemical method has been implemented in order to obtain Au@ZnO HNs. The synthesized HNs consist in 40 nm mean size almost spherical Au NPs cores, over which the heterogeneous formation of ZnO is observed. It was found that the morphology of the semiconductor material deposited over the core particles depends on the experimental conditions. In turn, these morphological changes induce significant modifications on the extinction spectra, which have been rationalized by means of two different electro-dynamics approaches: the Mie theory for coated spheres and the DDA method. In both cases an effective medium theory was used to describe the dielectric constant of the shell. The good

correlation between experimental and theoretical spectra indicates that the ZnO material that surrounds the Au core NP includes a significant amount of water. By implementing a graphical method to analyze the extinction spectra obtained by means of the exact extended Mie theory, it was possible to perform an accurate estimation of the main morphological parameters of the synthesized HNs. In addition, the DDA method was employed to address particularly the effect of the shape of the shell on the optical response of the HNs. By considering the shape of the surrounding material in a more realistic way within the DDA method, it was possible to estimate its water content, a parameter that could be rather hard to obtain by others approach.

## Methodologies

### Experimental methods

**Materials.** Sodium citrate (Na<sub>3</sub>C<sub>6</sub>H<sub>5</sub>O<sub>7</sub>, Mallinckrodt), chloroauric acid (HAuCl<sub>4</sub>, Carlo Erba), zinc nitrate (Zn(NO<sub>3</sub>)<sub>2</sub>·6H<sub>2</sub>O, Anedra) and potassium hydroxide (KOH, Cicarelli) were used as received without further purification. Aqueous solutions were prepared with ultrapure water (18.2 mΩ resistivity).

**Synthesis of Au NPs.** Nearly spherical Au NPs of mean size 40 nm were obtained according to the Turkevich method. Aliquots of 0.1 M sodium citrate aqueous solution (0.25 mL) and of 0.01 M acid chloroauric aqueous solution (2.5 mL) were added to 97.25 mL of boiling water under vigorous stirring. After 2–3 minutes of reaction an intense red wine color was observed indicating the formation of Au NPs. The system was kept at boiling temperature during 5 minutes to complete reaction and then it was cooled at room temperature. Au NPs were purified by performing centrifugation of 13 mL of the aqueous suspension of Au NPs during 10 minutes at 5000 rpm. The resulting precipitate was redispersed in 12 mL of 3.33 mM KOH aqueous solution. The alkaline dispersion of Au NPs was then separated in four aliquots (A, B, C, D) of 3 mL each one.

**Synthesis of Au@ZnO HNs.** By implementing a very simple chemical methodology HNs dispersed in aqueous media were obtained. To each one of the 3 mL Au NPs alkaline dispersions (aliquots A, B, C and D), 2 mL of zinc nitrate aqueous solution of a certain concentration was added in order to obtain samples with increasing Zn(NO<sub>3</sub>)<sub>2</sub> concentration as displayed in Table 1. Note that 2 mL of water ([Zn(NO<sub>3</sub>)<sub>2</sub>] = 0 mM) were added to aliquot A in order to have an unmodified Au NPs sample as a control experiment. After adding the zinc nitrate solution, each one of the 5 mL volume samples A, B, C and D were kept at 80 °C

**Table 1** Zn(NO<sub>3</sub>)<sub>2</sub> and KOH concentrations employed in each different sample

Sample	Volume/mL	[Zn(NO <sub>3</sub> ) <sub>2</sub> ]/mM	[KOH]/mM
A	5	0.0	2.0
B	5	0.1	2.0
C	5	0.5	2.0
D	5	1.0	2.0

during 15 minutes and, finally cooled and stored at room temperature.

**Optical and morphological characterization.** UV-vis spectroscopy characterization was performed using a Shimadzu UV-1700 PharmaSpec spectrophotometer with a 1 cm quartz cell at room temperature. To determine the mean size (Z-average diameter) and the particle size distribution, photon correlation spectroscopy (PCS) measurements were performed with a DelsaNano C Particle Analyzer Beckman Coulter instrument using a 1 cm quartz cell at room temperature. Transmission electron microscopy (TEM) images were obtained using a JEM-JEOL 1120 EXII instrument under an accelerating voltage of 80 kV. Samples were prepared by seeding a drop ( $\sim 20 \mu\text{L}$ ) of the colloidal dispersion to be characterized onto a holey carbon/formvar-coated copper TEM grid (100 mesh).

**XRD characterization.** The XRD instrument employed was a PANalytical X-Pert Pro using a Cu K $\alpha$  radiation ( $\lambda = 1.5406 \text{ \AA}$ ). The diffractograms were obtained in the range  $30\text{--}70^\circ$  from powders of the particles. The respective powders were obtained by depositing droplets containing the nanostructures over glass slides, and evaporating the solvent in a fumehood at room temperature.

## Theoretical methods

**Mie theory for coated spheres.** A complete and detailed description of this method can be found in the book written by Bohren and Huffman.<sup>37</sup> This theory constitutes an exact solution to the problem of absorption and scattering of light by an object composed by concentric spheres. We have used the BHCOAT code, which implements such a solution, to simulate the extinction properties of Ag@ZnO core shell NHs.

**DDA method.** Details about this methodology can be found elsewhere.<sup>38–41</sup> Briefly, this approximated method allows the calculation of the optical properties of arbitrarily shaped objects with a high degree of accuracy. In this method, the continuum target, *i.e.* the nanostructure, is approximated by a cubic array of  $N$  polarizable elements (dipoles) at positions  $r_i$  with dipole polarizabilities  $\alpha_i$ . Due to the freedom to locate dipoles at any site of the cubic array, it is possible to model the optical properties of arbitrarily shaped objects with domains having different compositions. The dielectric constant of each material forming the target  $\epsilon(\lambda)$  is introduced externally is input, and the method employs the lattice dispersion relation to determine the  $\alpha_i$  values so that an infinite array with finite lattice spacing mimic an extended solid with dielectric constant  $\epsilon(\lambda)$ .<sup>42</sup> Furthermore, the number of dipoles used to represent a given particle can be thought as a control parameter of the code. By increasing the dipole number, the accuracy of the calculation is improved as well as the computational time increases. The number of dipoles used in the calculations should be chosen in such a way that convergence has been reached. In this work, we have used the DDSCAT 7.3 code to simulate the optical response of Au@ZnO NHs.<sup>43</sup> A lattice spacing (inter dipole distance) of 1.33 nm was used in all simulations whereas the total number of dipoles to represent the target was kept in the range  $726\,744 \pm 63$ .

## Results and discussion

### Experimental extinction spectra of Au@ZnO HN

Fig. 1 shows the extinction spectra of suspensions of Au@ZnO HN synthesized according to the procedure described above. The extinction spectrum of the unmodified Au NPs colloidal dispersion (black curve), which correspond to  $[\text{Zn}(\text{NO}_3)_2] = 0.0 \text{ mM}$ , resembles the typical spectrum expected for this system, exhibiting a peak centered at 528 nm which is attributed to the excitation of the Au NPs LSPR. When a  $[\text{Zn}(\text{NO}_3)_2]$  of 0.1 mM was used in the synthesis (red curve), the LSPR peak position slightly red shifts 2 nm being centered at 530 nm, while a moderate increase in the extinction intensity for wavelength ( $\lambda$ ) values shorter than 380 nm is observed in comparison with the previous case (black curve,  $[\text{Zn}(\text{NO}_3)_2] = 0.0 \text{ mM}$ ).

These changes are more important when the  $[\text{Zn}(\text{NO}_3)_2]$  employed in the experiment is 0.5 mM (green curve). In this case, the LSPR peak increases its intensity and appears centered at 540 nm, while the extinction intensity for  $\lambda$  values shorter than 380 nm is noticeably amplified and exhibit a shoulder at 350 nm. More pronounced changes are observed for the case of HN synthesized with  $[\text{Zn}(\text{NO}_3)_2] = 1.0 \text{ mM}$  (blue curve): the intensity of the LSPR is increased and the peak red-shifts to 550 nm whereas the extinction intensity in the UV region is enlarged almost four times with respect to the spectrum of the naked Au NPs and displays a defined shoulder at 350 nm. The description of the main phenomena suggests that the remarkable enlargement of the extinction intensity in the UV region, particularly for  $\lambda$  values around 350 nm, is consistent with the absorption features of ZnO. On the other hand, the considerable redshifts of the LSPR peak position can be attributed, in principle, to two principal causes: plasmonic coupling between Au NPs or increase of the dielectric constant of the environment where the NPs are located. It is noteworthy that these two phenomena may occur simultaneously.

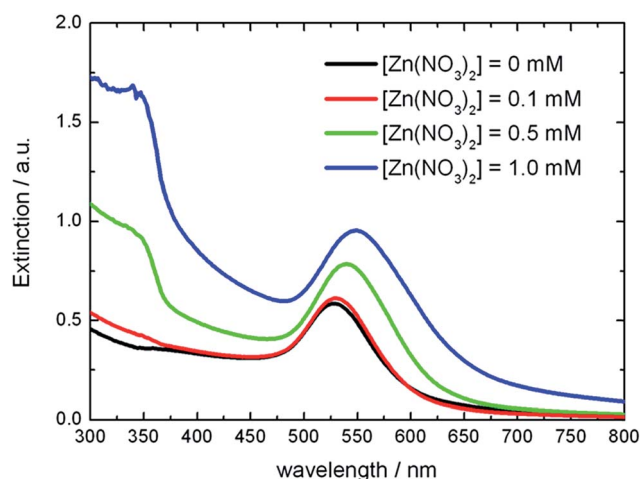


Fig. 1 Extinction spectra of Au@ZnO HN suspensions obtained for different concentrations of  $\text{Zn}(\text{NO}_3)_2$  employed in the synthesis as indicated in the inset.

### Morphological characterization of Au@ZnO HNs

Fig. 2 shows representative TEM images of the HNs obtained for  $\text{Zn}(\text{NO}_3)_2$  concentrations of (a) 0.0, (b) 0.1, (c) 0.5 and (d) 1.0 mM (samples A, B, C and D respectively). TEM images of the sample containing the unmodified Au NPs cores, *i.e.* Au NPs obtained by means of the Turkevich method, which were then purified by centrifugation, redispersed in basic media and heated at 80 °C during 15 minutes, are shown in Fig. 2a. It is observed that, in the absence of  $\text{Zn}^{2+}$ , nearly spherical Au NPs with mean size 40 nm were obtained. Note that the Au NPs size and shape distributions that can be appreciated from Fig. 2a is consistent with the extinction spectrum of the sample shown in Fig. 1 (black curve). More detailed information on the initial particle size distribution used for growing the HNs, was obtained by performing PCS measurements of unmodified Au NPs suspensions. The intensity size distribution obtained is shown in Fig. S1,<sup>†</sup> which presents a single peak centered at 45 nm, indicating that the hydrodynamic radius and the particle size distribution is consistent with the morphological information obtained by TEM. The TEM images shown in Fig. 2b–d clearly reveal the appearance of a different material closely connected to the Au NPs ascribed as ZnO. In the TEM image shown in Fig. 2b, this material is visualized as protuberances or branches that arise from the Au NPs surface. The number of branches in each Au NP varies between 2 and 6, being 50 nm its mean length. Qualitatively, similar HNs were obtained for  $[\text{Zn}(\text{NO}_3)_2] = 0.5$  mM (Fig. 2c). The TEM image corresponding to sample D (Fig. 2d), obtained with  $[\text{Zn}(\text{NO}_3)_2] = 1.0$  mM, shows qualitatively similar HNs, but in this case a considerably larger amount of ZnO attached to the Au NPs is observed in comparison with the HNs obtained with lower  $[\text{Zn}(\text{NO}_3)_2]$  values. Furthermore, the Au NPs appears as immersed into a ZnO matrix that resemble a shell which mean thickness is approximately 60 nm. It can be noted in the respective TEM images that the amount of ZnO that surrounds the Au cores increases proportionally to the  $\text{Zn}^{2+}$  concentration used in each experiment. Concomitantly, the width of the ZnO shell remains roughly at a constant value around 60 nm. Besides, irrespective of the  $[\text{Zn}(\text{NO}_3)_2]$  used, the mean size of the Au NPs is 40 nm and its size and shape distributions are practically the same to that observed in Fig. 2a for the naked Au NPs. This observation suggests that the Au NPs are not modified by adding  $\text{Zn}^{2+}$  or by increasing temperature. Furthermore, aggregation of Au NPs, which could lead to plasmonic coupling, and, consequently, to a red-shift of the extinction peaks, is not appreciated in these images.

In general, the TEM analysis indicates that the synthesized HNs display a flower-like morphology and that the degree of coverage of the Au core NPs by ZnO increases with the value of  $[\text{Zn}(\text{NO}_3)_2]$  employed in the synthesis. Importantly, the TEM images also show that, in all cases, the ZnO formation uniquely takes place on the Au NPs surface. This observation suggests that the Au NPs behave as nucleation centers for the heterogeneous precipitation of ZnO, and provides evidence that the LSPR redshift can be attributed to an increase of the local dielectric constant generated by oxide material that surrounds the Au NPs. Therefore, the

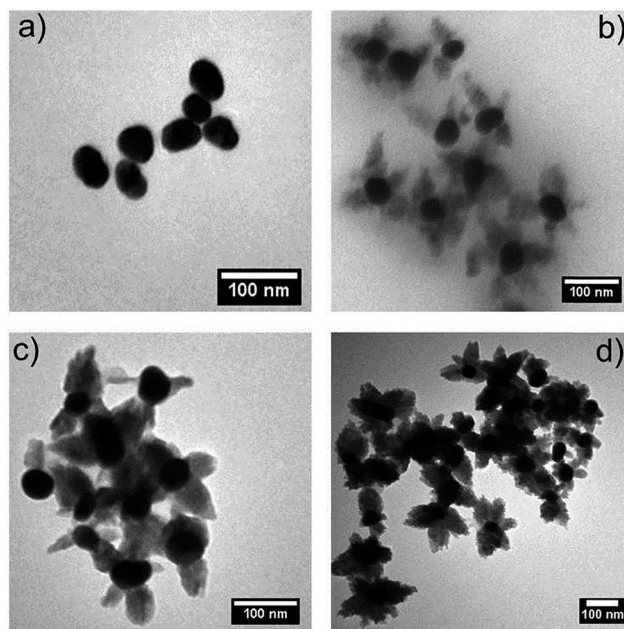


Fig. 2 Representative TEM images of the as-prepared Au@ZnO HNs obtained for different concentrations of  $\text{Zn}(\text{NO}_3)_2$  employed in the synthesis: (a) 0.0 mM, (b) 0.1 mM, (c) 0.5 mM and (d) 1.0 mM.

morphological characteristics of the HNs revealed by the TEM images analysis are in a quite good qualitative agreement with the interpretation regarding the changes observed in the extinction spectra.

### XRD characterization

Fig. 3 shows the XRD patterns of the powders obtained from the unmodified Au NPs and from the Au@ZnO HNs (synthesized with  $[\text{Zn}(\text{NO}_3)_2] = 1.0$  mM) denoted as (a) and (b), respectively. For comparison, the standard data for fcc metal Au (JCPDS 4-784) and hexagonal wurtzite ZnO (JCPDS 36-1451) are also shown at the bottom as blue and red bars, respectively.

The diffraction pattern of Au NPs shows three peaks at  $2\theta = 38.2, 44.4$  and  $64.6$ , which are assigned to the reflections of the planes (111), (200) and (220) of Au, respectively. On the other hand, the diffraction pattern of Au@ZnO HNs shows peaks at  $2\theta = 31.7, 34.4, 36.3, 56.7, 62.9$  and  $68.0$  which are assigned to the reflections of the planes (100), (002), (101), (110), (103) and (112) of ZnO, respectively, in addition to the peaks attributed to reflections of the Au phase. The background signal, particularly its increase for  $2\theta \rightarrow 30$ , is attributed to amorphous  $\text{SiO}_2$  (JCPDS 29-0085) which constitutes the material employed to support the sample during measurements, whereas the additional peaks present in the Au@ZnO HNs pattern at  $2\theta = 31.7, 34.4$  might be assigned to reflections of the planes (102) and (211) of Quartz (JCPDS 33-1161). Therefore, these results confirm the formation of an irregular ZnO shell on the Au cores, and further support the interpretation of the measured changes in the optical properties. Furthermore, the Scherrer equation (see ESI<sup>†</sup>) was applied to estimate the crystallite size of the respective materials (instrumental broadening was considered negligible and

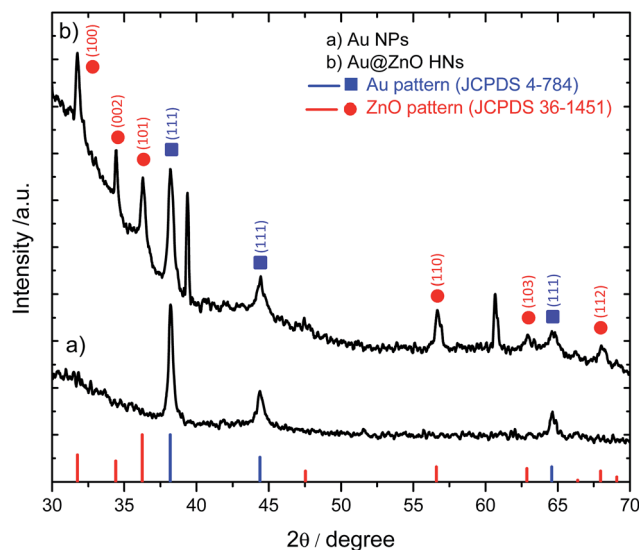


Fig. 3 XRD patterns of (a) Au NPs and (b) Au@ZnO HNs. The reference XRD pattern of Au (JCPDS 4-784) and ZnO (JCPDS 36-1451) are also shown in the lower part of the figure as blue and red bars, respectively. The patterns have been arbitrarily shifted in the y-axis.

was not included in the analysis). In particular for Au NPs, the mean coherence length perpendicular to the planes (111) gives a value of 26 nm, while for ZnO the mean coherence length perpendicular to the planes (101) gives a value of 24 nm.

### Modelling of the extinction spectra of HNs

Probably the simplest model to describe the optical response of the synthesized HNs is graphically schematized in Fig. 4. It consists in two concentric spheres: a Au core of diameter  $D$  surrounded by a uniform shell of thickness  $S$  dispersed in water.

Note that the composition of the shell is heterogeneous as it is composed by water and ZnO. Thus, the simple proposed model aims to capture the most relevant morphological features observed in the TEM images. The extinction spectrum of the proposed concentric spheres model to describe the optical response of the synthesized HNs, can be exactly

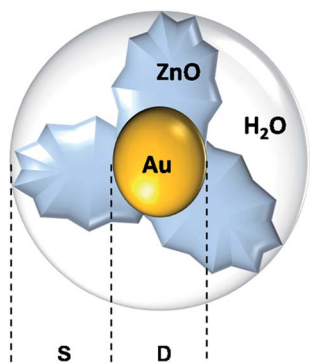


Fig. 4 Graphic scheme of the model used in Mie theory for coated spheres simulations to represent the synthesized Au@ZnO HNs.

calculated in the frame of classical electrodynamics by using the Mie theory for coated spheres as formulated by Aden and Kerker (ref. 37, page 181). The dielectric constants of the Au core as well as of the shell are essential quantities in order to perform such simulations. The dielectric constant of the core (Au) was obtained from literature<sup>44</sup> whereas the dielectric constant of the shell was obtained by means of effective-medium theories. In this case, the expression reported by Garnett (ref. 37, page 217) has been employed to determine the dielectric constant of the shell  $\epsilon_{\text{eff}}$ :

$$\epsilon_{\text{eff}} = \epsilon_m \left[ 1 + \frac{3f \left( \frac{\epsilon - \epsilon_m}{\epsilon + 2\epsilon_m} \right)}{1 - f \left( \frac{\epsilon - \epsilon_m}{\epsilon + 2\epsilon_m} \right)} \right] \quad (1)$$

where  $\epsilon$  stands for the dielectric constant of ZnO (which was obtained from the values reported by Postava *et al.*<sup>45</sup>),  $\epsilon_m$  ( $= 1.33$ ) the dielectric constant of water and  $f$  the filling factor defined as the ratio of the volume of the shell occupied by ZnO to the total volume of the shell. The simulated extinction efficiency spectra  $Q_{\text{ext}}$  of Au@ZnO HNs with fixed geometrical parameters ( $D = 40$  nm,  $S = 50$  nm) calculated according to the approach described above are shown in Fig. 5a. In this set of spectra the filling factor  $f$  is varied from 0 to 0.8. Qualitatively, it can be clearly observed that as the  $f$  values increase from 0 to 0.8, the changes in the extinction spectra are quite similar to those observed in the measured extinction spectra (see Fig. 1). On the one hand, a large increase of the extinction intensity in the UV region particularly for  $\lambda$  values around 350 nm is observed, where the shoulder located at around 350 nm appears as a clearly defined peak as the value of  $f \rightarrow 1$ . This increase of the extinction in the UV region is attributed to the increasing fraction of ZnO that compose the shell of the HNs. On the other hand, a substantial red-shift of the Au NP LSPR from 530 to 590 nm when the  $f$  value increases from 0 to 0.8 is observed. This redshift is attributed to an increase of the dielectric constant of the environment where the Au core is located as the filling factor  $f \rightarrow 1$ . Fig. 5b shows the effect of increasing the shell thickness on the simulated extinction spectra of Au@ZnO HNs with fixed diameter and filling factor  $f$  values ( $D = 40$  nm,  $f = 0.3$ ). In this case, qualitatively similar changes to those described in Fig. 5a are found: a large increase of the extinction intensity in the UV region as well as a noticeable red-shift of the Au NP LSPR. However, the magnitude of the LSPR redshift observed in Fig. 5b, from 530 to 550 nm when the  $S$  value increases from 0 to 80 nm, is almost a half in comparison to that observed in Fig. 5a. In addition, note that the LSPR red-shift from 545 to 550 nm when the  $S$  value increases from 20 to 80 nm, for a constant  $f = 0.3$  value. This fact indicates that the value of the dielectric constant of the environment experienced by the Au core is more sensitive to the filling factor  $f$  value than to the shell thickness.

Fig. 6 summarize the main features of the simulated spectra shown in Fig. 5 along with the respective data for other not shown spectra corresponding to HNs with different geometries. Fig. 6a shows the variation of the LSPR spectral position ( $\lambda_{\text{res}}$ ) with the filling factor  $f$  for several shell thickness  $S$ . For a given

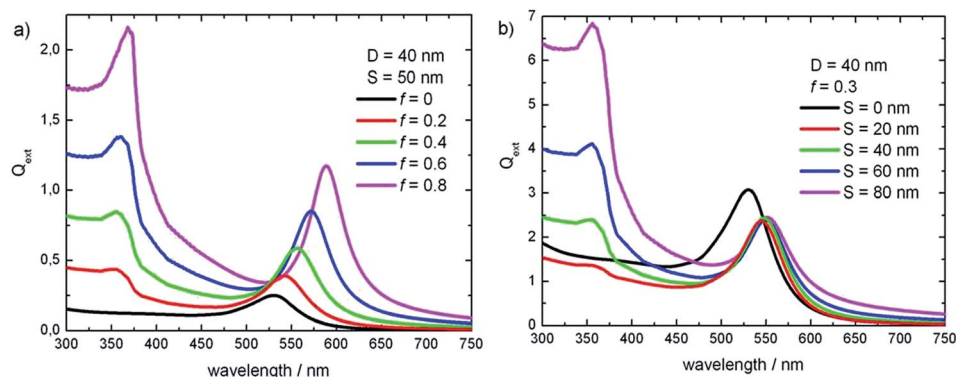


Fig. 5 Effects of (a) filling factor  $f$  and (b) shell thickness  $S$  on the simulated extinction efficiency spectra  $Q_{\text{ext}}$  of Au@ZnO HNs according to the Mie theory for coated spheres.

thickness, it is observed that  $\lambda_{\text{res}}$  varies almost linearly with  $f$ . In addition, for a given  $f$  value, the sensitivity of  $\lambda_{\text{res}}$  upon a thickness change is inversely proportional to the shell size. For instance, for  $f = 0.5$ ,  $\lambda_{\text{res}}$  changes from 530 to 550 nm ( $\Delta\lambda_{\text{res}} = 20$  nm) when  $S$  increases from 10 to 20 nm ( $\Delta S = 10$  nm). However,  $\lambda_{\text{res}}$  changes from 550 to 560 nm ( $\Delta\lambda_{\text{res}} = 10$  nm) when  $S$  increases from 20 to 30 nm ( $\Delta S = 10$  nm). Moreover,  $\lambda_{\text{res}}$  changes from 563.5 to 565 nm ( $\Delta\lambda_{\text{res}} = 1.5$  nm) when  $S$  increases from 50 to 60 nm ( $\Delta S = 10$  nm). This trend strongly suggests that the magnitude of the redshift of the LSPR is mostly determined by the properties of the adjacent environment to the Au core NP. Fig. 6b shows the magnitude of the parameter  $R$  defined as the ratio between the values of the extinction efficiency  $Q_{\text{ext}}$  evaluated at  $\lambda_{\text{res}}$  to the value of  $Q_{\text{ext}}$  evaluated at 350 nm vs.  $f$ , for several shell thickness  $S$  values. In these set of curves it can be observed that the relation between  $R$  and  $f$  is largely influenced by the shell thickness. For  $S = 10$  nm, the values of  $R$  increase with  $f$ , which implies that the extinction at  $\lambda_{\text{res}}$  is higher with respect to that at 350 nm. On the contrary, the opposite trend is found for  $S \geq 30$  nm.

The spectral information summarized in Fig. 6 can be used as an accurate guide to obtain information about the morphology of the experimentally prepared Au@ZnO HNs. Note

that both quantities  $\lambda_{\text{res}}$  and  $R$  are easily accessible experimentally by means of extinction measurements. If considered the sample obtained with  $[\text{Zn}(\text{NO}_3)_2] = 1.0$  mM, it is found that its characteristic spectral values are  $\lambda_{\text{res}} = 549$  nm and  $R = 0.58$ . These parameters can be used along with Fig. 6 to estimate the average shell thickness  $S$  and the filling factor  $f$  for this sample. It can be noted from Fig. 6a that there are a large number of different combinations between  $S$  and  $f$  values that present  $\lambda_{\text{res}} = 549$  nm, for instance,  $S = 10$  nm and  $f = 0.5$  as well as  $S = 50$  nm and  $f = 0.3$  (the black dot line at  $\lambda = 549$  nm it is plotted to guide the eye). On the other hand, it can also be observed from Fig. 6b that there are a large number of different combinations between  $S$  and  $f$  values that present  $R = 0.58$  (see the black dot line at  $R = 0.58$ ). However, there is a unique set of  $S$  and  $f$  values that simultaneously match the  $\lambda_{\text{res}} = 549$  nm and  $R = 0.58$  values. In the case under consideration, these values are  $S = 61$  nm and  $f = 0.29$ . It is possible to perform the same procedure for the experimentally obtained  $\lambda_{\text{res}}$  and  $R$  values corresponding to samples A, B and C, and determine its morphological parameters  $S$  and  $f$  associated. Fig. 7 show the extinction spectra simulated with the  $S$  and  $f$  values obtained for each sample according to the procedure described above.

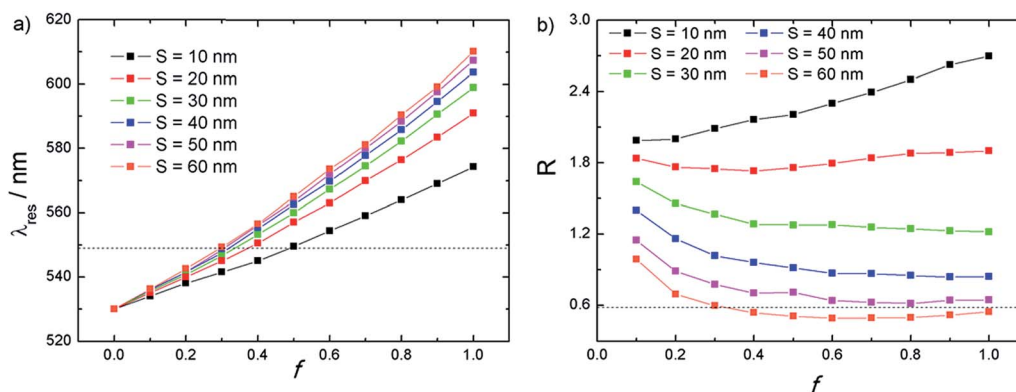


Fig. 6 Variation of the simulated (a)  $\lambda_{\text{res}}$  and (b)  $R$  values with filling factor  $f$  for different shell thickness  $S$  according to the Mie theory for coated spheres.

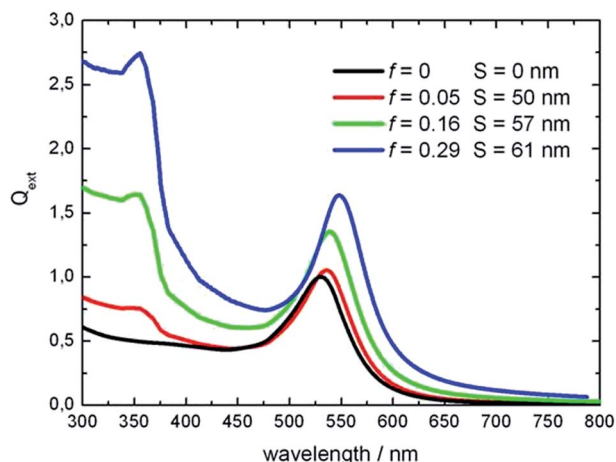


Fig. 7 Au@ZnO HNs simulated extinction efficiency spectra with the  $f$  and  $S$  values described in the inset. In all cases the diameter of the Au core NP is 40 nm.

It is found that the computational results obtained exhibit a very good qualitative as well as quantitative agreement with the experimentally measured spectra (Fig. 1). Importantly, note that the  $S$  and  $f$  values obtained for each sample are in close agreement with the morphologies that can be appreciated from the TEM images (Fig. 2). This comparison shows that the optical response of the Au@ZnO HNs chemically synthesized can be accurately described by means of a coated sphere model along with effective medium theory to represent the dielectric constant of the ZnO shell.

To obtain further insight into the optical properties of the HNs we have also performed DDA simulations. This versatile and powerful methodology allows simulate the optical properties of nanostructures with arbitrary composition and geometry, at difference with the Mie theory which is restricted to spherical shaped particles. Therefore we employed it to address in particular the effect of the shape of the material that surrounds the Au core NP on the optical response of the HNs. Specifically, focus has been made in simulate the optical properties of the HNs obtained when a  $[\text{Zn}(\text{NO}_3)_2] = 1.0$  mM concentration was used in the experiments (Fig. 1, blue curve). The schemes shown in Fig. 8 illustrates some of the nanostructures computationally generated to calculate its extinction properties, which describe the synthesized HNs in a more approximate way than the core shell structures, and consist in a 40 nm diameter Au core NP located at the intersection between a given number of ellipsoids, whose number range from 2 to 6 (note that Fig. 8 illustrates the HNs composed by 2, 3 and 4 ellipsoids). More specifically, the 40 nm diameter Au core was represented by 14 147 dipoles arranged in a spherical way in all cases. The code applies the lattice dispersion relation to determine the  $\alpha_i$  values of the 14 147 dipoles so that an infinite array mimic the dielectric constant  $\epsilon(\lambda)$  of Au bulk.<sup>44</sup> On the other hand, the surrounding material was described by  $712\,597 \pm 63$  dipoles arranged in the volume defined between the external surface of the ellipsoids and the Au core.

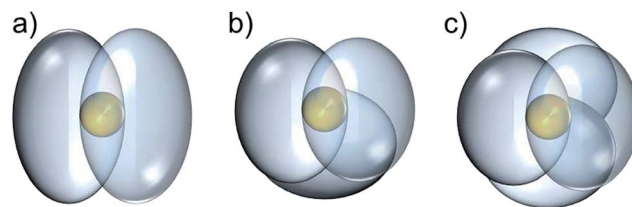


Fig. 8 Schemes of the structures employed in the DDA method to simulate the extinction spectra of the synthesized HNs, which consist in a 40 nm diameter Au core NP at the intersection between (a) 2, (b) 3 and (c) 4 ellipsoids, respectively.

In addition, the dimensions of the ellipsoids in each case (see Table 2) were determined in order that the volume occupied by them keeps constant and equal to  $1.69 \times 10^6 \text{ nm}^3$ . Besides, in each case the volume of these nanostructures is contained within a sphere of 80 nm radius. The effective medium theory was used to obtain the dielectric constant of the material surrounding the Au core NP, *i.e.* the ellipsoids, using a  $f_{\text{DDA}} = 0.35$  value. Note that this  $f_{\text{DDA}} (= 0.35)$  value should not be directly compared with the  $f (= 0.29)$  value employed in the Mie theory simulations because, although the ZnO volume is essentially the same in both cases, it is referred to different total volumes:  $2.11 \times 10^6 \text{ nm}^3$  for the case of the spherical shell in the Mie theory simulations, whereas to  $1.69 \times 10^6 \text{ nm}^3$  for the case of the ellipsoids in the DDA method. In other words, the total volume is reduced when changing the morphology from a spherical shell to the other one less regular defined by the ellipsoids, therefore the  $f$  value increases as stated by its definition. In order to obtain comparable  $f$  values, the following argument was employed to calculate the  $f_{\text{DDA}}$  value in relation to the volume of the spherical shell. In DDA simulations, the total volume occupied by the ellipsoids irrespective of its number ( $1.69 \times 10^6 \text{ nm}^3$ ) is represented by 712 650 dipoles, and considering the  $f_{\text{DDA}} = 0.35$  value, it can be thought that 249 427 dipoles represents the ZnO material.<sup>46</sup> On the other hand, the total volume occupied by the spherical shell ( $2.11 \times 10^6 \text{ nm}^3$ ) is represented by 890 781 dipoles. Thus, the ratio  $249\,427/890\,781$  gives a value of 0.28, which is quite similar to the  $f (= 0.29)$  value determined according to Mie theory simulations. It is important to note that, in this case, the DDA method applied the lattice relation dispersion to determine the polarizabilities of the dipoles that constitute the surrounding material so that an infinite array mimic the dielectric constant calculated using the effective medium theory given by eqn (1).

Fig. 9 shows the simulated extinction spectra for HNs with 2, 3, 4, 5 and 6 ellipsoids, where it can be appreciated that the main spectral features, *i.e.* a shoulder and a peak centered at

Table 2 Dimensions of the nanostructures employed in DDA calculations to simulate the extinction spectra of the synthesized HNs. In all cases the diameter of the core Au NP is 40 nm

Number of ellipsoids	2	3	4	5	6
Minor axes/nm	100	100	100	100	100
Major axes/nm	135	128	119	113	107

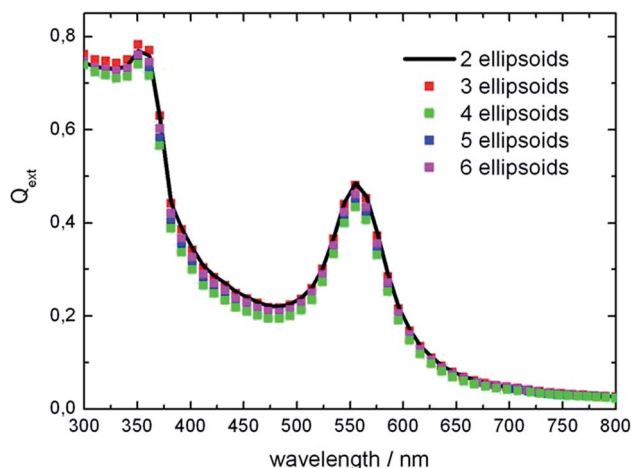


Fig. 9 DDA calculated extinction spectra of Au@ZnO HNs composed by a spherical Au core located at the intersection between different numbers of ZnO ellipsoids as indicated in the inset.

350 and 550 nm, respectively, clearly resemble the extinction spectrum of the HNs obtained for  $[\text{Zn}(\text{NO}_3)_2] = 1.0 \text{ mM}$  (Fig. 1, blue curve). In addition, the DDA simulated spectra are not affected by changing the shape of the material surrounding the Au core NP as this set of spectra significantly overlap. Importantly, the  $f_{\text{DDA}} = 0.35$  value employed in the simulations indicates that the precipitated material around the Au core contain a relatively high amount of water (65%), and show a very good agreement with the  $f = 0.4$  value reported previously for Ag@ZnO core shell HNs synthesized by means of a similar methodology.<sup>35</sup> Note that within the DDA method a more realistic representation of the morphology of the synthesized HNs can be performed in comparison with the Mie approach, and, consequently, a more approximated value of the parameter  $f$  can be obtained.

## Conclusions

In this work a very simple chemical methodology has been implemented which allows to obtain Au@ZnO HNs in aqueous media. The HNs obtained consist in almost spherical Au core NPs, whose mean size is 40 nm, surrounded by an irregular ZnO shell. According to TEM images, the ZnO material appears as protuberances that merge from the Au NPs surface. The quantity of ZnO protuberances, which mean length is around 60 nm, vary between 2 and 6. The major effect of increasing the amount of  $[\text{Zn}(\text{NO}_3)_2]$  employed in the synthesis is to increase the value of the filling factor  $f$  of ZnO within the shell, rather than increase the shell thickness. We propose that the synthetic methodology implemented in this work can be easily applied to other Au NPs shape and shell material, broadening the possibilities of synthesizing HNs in aqueous media. In addition, as a consequence of the ZnO shell formation significant changes in the extinction spectra of the Au NPs were observed. These changes in the optical response have been rationalized by means of electrodynamics simulations based on two different approaches: the Mie theory for coated spheres and the discrete

dipole approximation. In both cases, the effective medium theory was used to describe the dielectric constant of the ZnO shell. The good correlation between experimental and theoretical spectra indicates that the model employed properly describes the optical response of Au@ZnO HNs. By implementing a graphical method to analyze the extinction spectra simulated with the Mie theory, it was possible to perform an accurate prediction of the main morphological parameters of the synthesized Au@ZnO HNs. In addition, the combination of DDA modeling with optical measurements and morphological information, allows estimate that the water content of the shell surrounding the metallic core is 65%. Lastly, we believe the methodology implemented in this work to study the optical properties of Au@ZnO HNs provides a useful tool to obtain, in addition, relevant structural information, which could also be applied to study other systems composed by different plasmonic and dielectric materials.

## Acknowledgements

The authors thank CONICET (PIP 112-201101-00430), FONCYT (PICT-2012-2286) and SECYT (UNC) for financial support. The authors thank Dra. Cecilia Blanco for technical assistance in XRD measurements.

## References

- 1 F. Chunga, Z. Zhub, P. Luo, R. Wua and W. Li, *Sens. Actuators, B*, 2014, **199**, 314–319.
- 2 Y. Chen, D. Zeng, K. Zhang, A. Lu, L. Wang and D. Peng, *Nanoscale*, 2014, **6**, 874–881.
- 3 C. Mondal, Y. Pal, M. Ganguly, A. K. Sinha, J. Jana and T. Pal, *New J. Chem.*, 2014, **38**, 2999–3005.
- 4 Y. Quab and X. Duan, *Chem. Soc. Rev.*, 2013, **42**, 2568–2580.
- 5 P. Li, Z. Wei, T. Wu, Q. Peng and Y. Li, *J. Am. Chem. Soc.*, 2011, **133**, 5660–5663.
- 6 X. Feng, G. Hu and J. Hu, *Nanoscale*, 2011, **3**, 2099–2117.
- 7 L. Zhang, L. Yin, C. Wang, N. Iun, Y. Qi and D. Xiang, *J. Phys. Chem. C*, 2010, **114**, 9651–9658.
- 8 E. R. Encina and E. A. Coronado, *J. Phys. Chem. C*, 2010, **114**, 3918–3923.
- 9 E. R. Encina and E. A. Coronado, *J. Phys. Chem. C*, 2007, **111**, 16796–16801.
- 10 M. Rycenga, C. M. Cobley, J. Zeng, W. Li, C. H. Moran, Q. Zhang, D. Qin and Y. Xia, *Chem. Rev.*, 2011, **111**, 3669–3712.
- 11 M. R. Jones, K. D. Osberg, R. J. Macfarlane, M. R. Langille and C. A. Mirkin, *Chem. Rev.*, 2011, **111**, 3736–3827.
- 12 Z. Zhuang, Q. Peng and Y. Li, *Chem. Soc. Rev.*, 2011, **40**, 5492–5513.
- 13 J. Watt, S. Cheong and R. D. Tilley, *Nano Today*, 2013, **8**, 198–215.
- 14 M. R. Buck and R. E. Schaak, *Angew. Chem.*, 2013, **52**, 6154–6178.
- 15 Y. Chen, K. Munechika, I. Jen-La Plante, A. M. Munro, A. M. Skrabalak, Y. Xia and D. S. Ginger, *Appl. Phys. Lett.*, 2008, **93**, 053106.

- 16 K. Munechika, Y. Chen, A. F. Tillack, A. P. Kulkarni, I. Jen-La Plante, A. M. Munro and D. S. Ginger, *Nano Lett.*, 2010, **10**, 2598–2603.
- 17 T. Torimoto, H. Horibe, T. Kameyama, K. Okazaki, S. Ikeda, M. Matsumura, A. Ishikawa and H. Ishihara, *J. Phys. Chem. Lett.*, 2011, **2**, 2057–2062.
- 18 M. Li, S. K. Cushing, Q. Wang, X. Shi, L. A. Hornak, Z. Hong and N. Wu, *J. Phys. Chem. Lett.*, 2011, **2**, 2125–2129.
- 19 H. Naiki, A. Masuhara, S. Masuo, T. Onodera, H. Kasai and H. Oikawa, *J. Phys. Chem. C*, 2013, **117**, 2455–2459.
- 20 P. Viste, J. Plain, R. Jaffiol, A. Vial, P. M. Adam and P. Royer, *ACS Nano*, 2010, **4**, 759–764.
- 21 A. Wood, M. Giersig and P. Mulvaney, *J. Phys. Chem. B*, 2001, **105**, 8810–8815.
- 22 V. Subramanian, E. Wolf and P. V. Kamat, *J. Phys. Chem. B*, 2003, **107**, 7479–7485.
- 23 M. Jakob, H. Levanon and P. V. Kamat, *Nano Lett.*, 2003, **3**, 353–358.
- 24 J. Lee, H. S. Shim, M. Lee, J. K. Song and D. Lee, *J. Phys. Chem. Lett.*, 2011, **2**, 2840–2845.
- 25 Z. Sun, Z. Yang, J. Zhou, M. H. Yeung, W. Ni, H. Wu and J. Wang, *Angew. Chem., Int. Ed.*, 2009, **48**, 2881–2885.
- 26 J. Zhang, J. Tang, K. Lee and M. Ouyang, *Science*, 2010, **327**, 1634–1638.
- 27 N. Zhang, S. Liu, X. Fu and Y. Xu, *J. Phys. Chem. C*, 2011, **115**, 91369145.
- 28 Y. Qin, Y. Zhou, J. Li, J. Maa, D. Shi, J. Chen and J. Yang, *J. Colloid Interface Sci.*, 2014, **418**, 171–177.
- 29 K. K. Haldar, T. Sen and A. Patra, *J. Phys. Chem. C*, 2008, **112**, 11650–11656.
- 30 N. P. Herring, K. A. Zeid, M. B. Mohamed, J. Pinski and M. S. El-Shall, *Langmuir*, 2011, **27**, 15146–15154.
- 31 D. Liu, S. Ding, H. Lin, B. Liu, Z. Ye, F. Fan, B. Ren and Z. Tian, *J. Phys. Chem. C*, 2012, **116**, 4477–4483.
- 32 L. Zhang, D. A. Blom and H. Wang, *Chem. Mater.*, 2011, **23**, 4587–4598.
- 33 L. Zhang, H. Jing, G. Boisvert, J. Z. He and H. Wang, *ACS Nano*, 2012, **6**, 3514–3527.
- 34 E. R. Encina, M. A. Pérez and E. A. Coronado, *J. Nanopart. Res.*, 2013, **15**, 1688.
- 35 K. Laaksonen, S. Suomela, S. R. Puisto, N. K. J. Rostedt, T. Ala-Nissila and R. M. Nieminen, *J. Opt. Soc. Am. B*, 2014, **31**, 494–502.
- 36 E. Shaviv, O. Schubert, M. Alves-Santos, G. Goldoni, R. Di Felice, F. Vallée, N. Del Fatti, U. Banin and C. Sönnichsen, *ACS Nano*, 2011, **5**, 4712–4719.
- 37 C. F. Bohren and D. R. Huffman, *Absorption and Scattering of Light by Small Particles*, Wiley-Interscience, New York, 1983.
- 38 K. L. Kelly, E. A. Coronado, L. L. Zhao and G. C. Schatz, *J. Phys. Chem. B*, 2003, **107**, 668–677.
- 39 E. M. Purcell and C. R. Pennypacker, *Astrophys. J.*, 1973, **186**, 705–714.
- 40 B. T. Draine, *Astrophys. J.*, 1988, **333**, 848–872.
- 41 B. T. Draine and P. J. Flatau, *J. Opt. Soc. Am.*, 1994, **11**, 1491–1499.
- 42 B. T. Draine and J. Goodman, *Astrophys. J.*, 1993, **405**, 685–697.
- 43 <http://code.google.com/p/ddscat/>.
- 44 *Handbook of Optical Constant of Solids*, ed. E. D. Palik, Academic Press, New York, 1985.
- 45 K. Postava, H. Sueki, M. Aoyama, T. Yamaguchi, C. Ino, Y. Igasaki and M. Horie, *J. Appl. Phys.*, 2000, **87**, 7820.
- 46 According to the inter dipole separation (1.333 nm) the volume corresponding to each dipole is 2.47 nm<sup>3</sup>.